# Closed-loop control of shear flows using real-time PIV

**Eliott Varon[1,2], Nicolas Gautier[1], Jean-Luc Aider[1,2,*]**

[1]Laboratoire PMMH, UMR7636 CNRS, ESPCI, 10 rue Vauquelin, 75005 Paris, France
[2]Paris Sciences Lettres (PSL⋆), 75005 Paris, France
[*]corresponding author: jean-luc.aider@espci.fr

**Abstract** A high-speed implementation on a Graphics Processor Unit (GPU) of an optical flow algorithm is used to compute in real time 2D2C (2-Components of the velocity fields in a 2D plane). The instantaneous state of the flow can then be estimated in real time and used as an input for closed-loop flow control experiments [9]. This novel approach has been applied to the Backward-Facing Step (BFS) flow. Two flow control experiments have been successfully implemented. The first one consists in monitoring in real-time the shedding frequency and actuating the incoming boundary layer at the same frequency [7]. The second one consists in searching a new closed-loop separation control using a machine learning algorithm [8]. All these examples confirm the great potential of Real-Time PIV for closed-flow control experiments as well as to accelerate the large parametric studies.
**Keywords:** Real-Time PIV, Closed-loop flow control, shear flows.

## 1 Introduction

In several domains such as aeronautics and thermodynamics, there is a high interest in controlling shear flows since convective instabilities will amplify the slightest disturbances while being advected downstream, increasing aerodynamic drag or decreasing combustion efficiency. The BFS flow is considered as a benchmark geometry for the shear flow study as separation is imposed by a sharp edge creating a strong shear layer susceptible to Kelvin-Helmholtz instability and a recirculation bubble where the stream-wise velocities are negative. Our control of the BFS flow aim at reducing the recirculation area. Kelvin-Helmholtz span-wise vortices shed in the shear layer downstream of the BFS at a frequency $f_{KH}$ strongly influence this area.
Three distinct approaches to flow control exists. Passive control involves permanent modifications of the geometry to yield the desired effect. Open-loop control modifies operating conditions of the system by supplying power to it. Finally closed-loop control improves open-loop control by using a feedback element to evaluate the flow state in order to compute appropriate commands and reject disturbances.

When considering closed-flow control, one has to choose the actuator that will induce perturbations in the flow and the sensor that will monitor the state of the flow. Usually, the sensors are wall pressure or wall shear-stress sensors which is a limitation to the possible closed-loop algorithm. Indeed, the wall sensors do not give access to all the characteristics of the flow, especially the coherent structures which are shed in the flow. To have access to volumic information, i.e. vortical structures created in the bulk of the flow, one has to use either hot-wire (HW) probe or Particle Image Velocimetry (PIV). HW probes induce perturbations and are not so well adapted for input in a closed-loop control. Up to now, PIV computation times were much too large to be used as an input in a closed-loop experiments. Recent progress in programmations of optical flow algorithms on GPUs allows Real-Time computations of of PIV velocity fields up to 100 Hz using a low-cost high-speed camera connected to a computer through a high-speed frame grabber [9]. We summarize in this paper the first applications of high-frequency real-time computations of PIV fields to closed-loop control experiments.

## 2 Experimental setup

### 2.1 Water tunnel

We conduct the experiments in a hydrodynamic channel in which the flow is driven by gravity and kept isothermal. Divergent and convergent sections separated by honeycombs ensure flow stabilisation. The test section is 80 cm long with a rectangular cross section 15 cm wide and 10 cm high. The quality of the main stream can be quantified in terms of flow uniformity and turbulence intensity. The standard deviation $\sigma$ is computed for the highest free-stream velocity $U_\infty$ featured in our experimental set-ups which is 22 cm.s$^{-1}$. We obtain $\sigma$ = 0.059 cm.s$^{-1}$ which corresponds to turbulence levels of $\sigma/U_\infty$ = 0.23%.

### 2.2 Backward-facing step geometry

In both BFS cases, a NACA 00019 leading-edge profile is used to smoothly start the boundary layer which then grows downstream along the flat plate, before reaching the edge of the step 33.5 cm downstream. The boundary layer is laminar and follows a Blasius profile. The Reynolds number $Re_h$ is based on the BFS height $h$ ($h = 1.5$ cm) and the free stream velocity $U_\infty$. As shown in figure 1, the channel height is $H = 7$ cm and the channel width is $W = 15$ cm. We can define the vertical expansion ratio $A_y = \frac{H}{H+h} = 0.82$ and the spanwise aspect ratio $A_y = \frac{w}{H+h} = 1.76$. In the Reynolds number range used in our experiments the largest mean recirculation length (length of the mean recirculation bubble shown on in Fig. 1) is $X_r = 6.75h$.

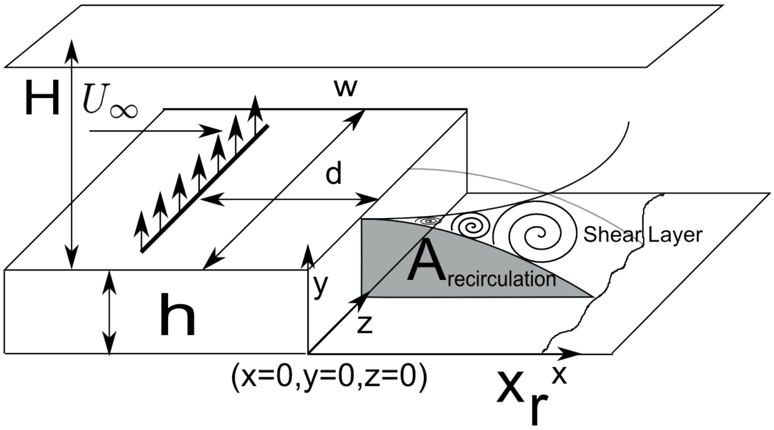


Fig. 1 Sketch of the BFS geometry and definition of the main parameters. From [7].

### 2.3 Actuator

It is a span-wise flush continuous slotted jet located at $d = 3.5$ cm = $2.3h$ upstream the step edge. The jet outlet has a rectangular cross-section which is 0.1 cm long (in the stream-wise direction) and 9 cm wide (span-wise direction). Injection is normal to the wall for the frequency-lock reactive control and makes an angle of 45° for the closed-loop separation control. A pressurized water tank, monitored by an electro-pneumatic regulator, is used to control the jet velocity $u_j$ as well as the actuation frequency $F_{act}$. The jet to cross-flow velocity ratio $a_0$ is defined as the ratio between the mean jet velocity $u_j$ and the free-stream velocity $U_\infty$ at a given Reynolds number $Re_h$: $a_0 = u_j/U_\infty$. The duty cycle is kept constant to $dc = 0.2$ when $F_{act}$ is used as a control parameter. This value for the duty-cycle was found optimal in a previous parametric study [6].

## 3 Real-Time PIV

The flow is seeded with 20 $\mu$m neutrally buoyant polyamid seeding particles. The vertical symmetry plane of the test section is illuminated by a laser sheet created by a 2 W continuous CW laser beam operating at wavelength $\lambda = 532$ nm passing through a cylindrical lens. A Basler acA 2000-340km 8bit CMOS camera record the pictures of the illuminated particles and transfer them to a computer through a camera-link NI PCIe 1433 frame grabber. Velocity fields are computed in real-time on the Graphics Processor Unit (GPU) of a Gforce GTX 580 graphics card.
The algorithm used to compute the velocity fields in the following experiments is a Lukas-Kanade optical flow algorithm called FOLKI and developed at ONERA [1]. The original images are reduced in size by a factor of 4 iteratively until intensity displacement in the reduced image is close to 0, giving a pyramid of images. The displacements are computed in the most reduced image with an initial guess of zero displacement using an iterative least-square Gauss-Newton minimization over a correlation window (20 px × 20 px). This displacement is then used as an initial estimate for the same scheme in the corresponding pair of images with a higher resolution in the pyramid. The process is repeated until the initial image, thus giving the final displacement. [3] and [9] give more details on this measurement method and rigorously demonstrate its offline and online

accuracy. The GPU version (FOLKI-GPU) was improved by Gautier & Aider [9] to allow for *real time and high frequency* computation of instantaneous velocity fields.
The size of the velocity fields is $(11.45 \times 3.0).h^2$ to capture the whole recirculation bubble. The sampling frequency for the real-time computed velocity fields is $f_s = 40$ Hz.

## 4 Frequency-lock reactive control of the BFS flow

### 4.1 Shedding frequency

Chun and Sung [4] have shown that forcing the shear layer close to its shedding frequency $f_{KH}$ is highly effective at reducing the recirculation bubble in separated flows. Thus a good input to a reactive control is $f_{KH}$ in order to set the actuator frequency $F_{act}$. As the shedding frequency depends on $Re_h(t)$, measuring $f_{KH}(t)$ in real time is fundamental to adapt properly $F_{act}$ to the flow.

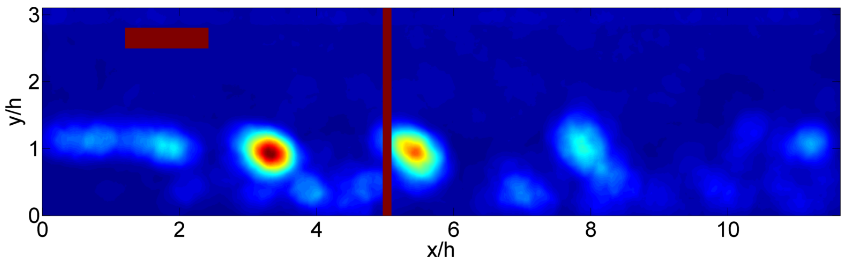


(a) Contours of $\lambda_{Ci}(x,y)$ at a given time step for $Re_h = 2800$. The *vertical line* shows the position where the $\lambda_{Ci}(5h,y)$ is integrated to identify shedding frequency. The *red rectangle* shows the position where flow velocity $u_{check}$ is computed.

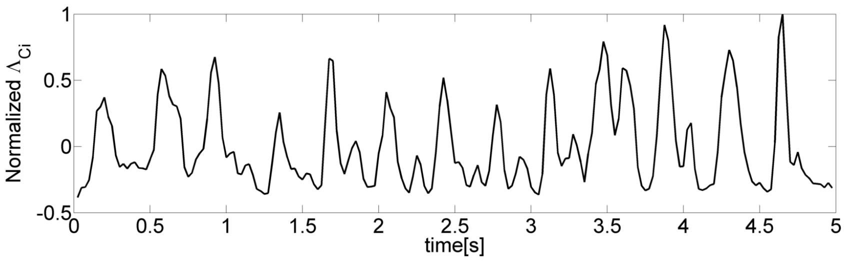


(b) $\Lambda_{Ci}$ time-series at $x_{det} = 5.0h$ for $Re_h = 2800$. Each peak corresponds to the passage of one vortex.

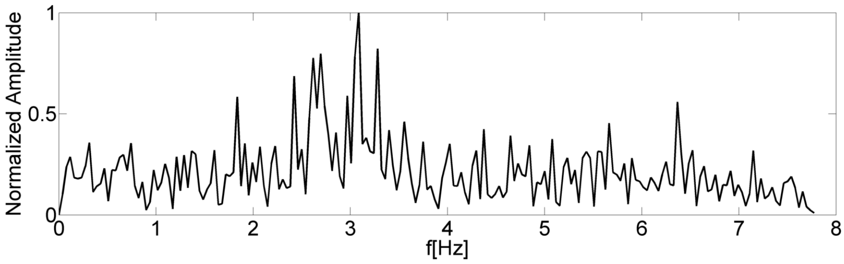


(c) Frequency spectrum for this time-series showing a stronger peak at $f_{KH} = 3.08$ Hz.

Fig. 2 Shedding frequency detection based on the swirling strength criterion $\lambda_{Ci}$. From [7].

Computing the 2D swirling strength criterion $\lambda_{Ci}(t)$ [2] in the velocity fields downstream of the step edge is an effective way to identify the vortices. Indeed when it is real $\lambda_{Ci}(t)$ is defined as:

$$\lambda_{Ci} = \frac{1}{2}\sqrt{4\det(\nabla\mathbf{u}) - \mathrm{tr}(\nabla\mathbf{u})^2} \tag{1}$$

and $\lambda_{Ci} = 0$ otherwise. An instantaneous snapshot of $\lambda_{Ci}(x,y)$ for $Re_h = 2800$ is shown on figure 2a, where

vortices are well visible. To know if $f_{KH}$ varies the changes in $Re_h$ are detected by continuously measuring $u_{check}(t)$, the spatially averaged upper corner of the stream-wise velocity field, located at the red rectangle position in the figure 2a, far from the boundaries.
Then the time-series of $\lambda_{Ci}(x,y,t)$ are spatially averaged in the vertical direction at $x_{det} = 5h$ position, highlighted by the red vertical line in the figure 2a, giving $\Lambda_{Ci}(t) = \langle \lambda_{Ci}(5h,t) \rangle_y$. Because the shear layer position depends also on the Reynolds number, $x_{det}$ is meticulously chosen such as the vortices detection stays valid and reliable whatever $Re_h$ is in these experiments. Figure 2b shows a typical time-series of fluctuations of normalized $\Lambda_{Ci}(t)$ for $Re_h = 2800$.
Finally a Fast Fourier Transform (FFT) of $\Lambda_{Ci}(t)$ enables to measure the shedding frequency corresponding to the time-series, giving here $f_{KH} = 3.08$ Hz, indicated by a sharp and well defined peak in the figure 2c. The robustness of the FFT mainly justifies this frequency identification method. As the real-time PIV enables an instantaneous access to the velocity fields and the computation of 2D $\lambda_{Ci}(t)$ is fast, the time to accurately obtain $f_{KH}$ depends only on the FFT length.

### 4.2 Optimal jet amplitude

The instantaneous recirculation area $A_{rec}(t)$ is computed to qualify the state of the flow as:

$$A_{rec}(t) = \int_{\mathscr{W}} H(-u(x,y,t))dxdy \tag{2}$$

where $\mathscr{W}$ is the real-time PIV window area, $H$ the Heaviside function, $u$ the stream-wise velocity. $A_{rec}(t)$ is then normalized by the time-averaged recirculation area for the uncontrolled flow $A_{0,Re_h}$. According to [6] the jet amplitude of the actuator can also be suitably chosen to improve the control of the BFS flow applying $F_{act} = f_{KH}$. Indeed $U_j$ has to be high enough to act on the flow but not too much to avoid high energy consumption. Thus the minimum seeking of $A_{rec}$, studied for a jet to cross-flow ratio $a_0 \leq 1.5$ at a given $Re_h$, leads to the optimal jet amplitude for this $Re_h$. After looking for the optimal values of $a_0$ at the extreme experiments Reynolds numbers (1400 and 2400), the other values are linearly interpolated to finally obtain $a_0$ as a function of $u_{check}$.

### 4.3 Control algorithm

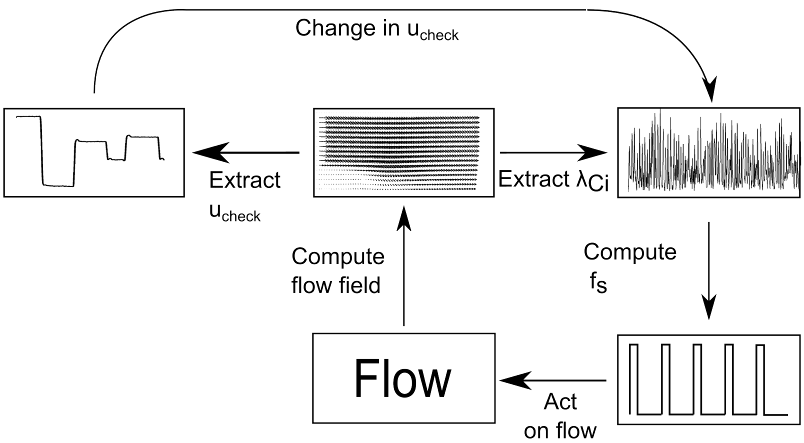


Fig. 3 Frequency-lock algorithm. From [7].

The reactive control algorithm is described in figure 3. When $u_{check}(t)$ does not vary for $\Delta T_{steady} = 5$ s, the actuation is turned off and $f_{KH}$ is computed over $\Delta T_{computation} = 20$ s with a relative difference of 5% compared to a computation over 30 min. Once the computation is done, the actuator starts to pulse the jet at $F_{act} = f_{KH}$ and at the optimal jet amplitude.

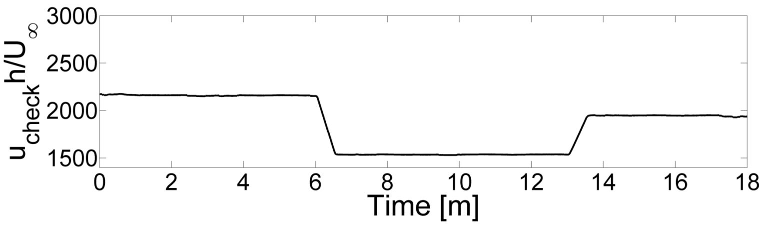


(a) Random variations of the Reynolds number $Re_h$, observed by $u_{check}$, as a function of time

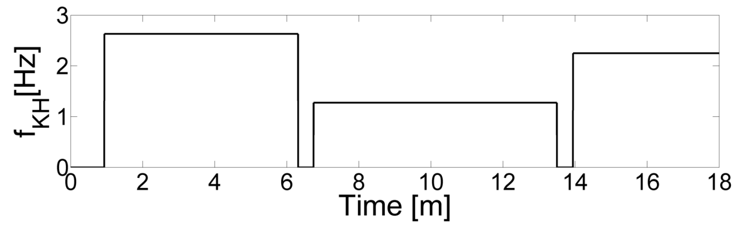


(b) Corresponding evolution of $f_{KH}$ as a function of time, following the variations of $Re_h(t)$.

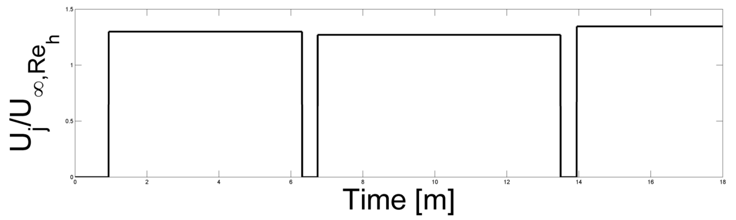


(c) Evolution of jet to cross-flow ratio amplitude $U_j/U_{\infty,Re_h}$ as a function of time.

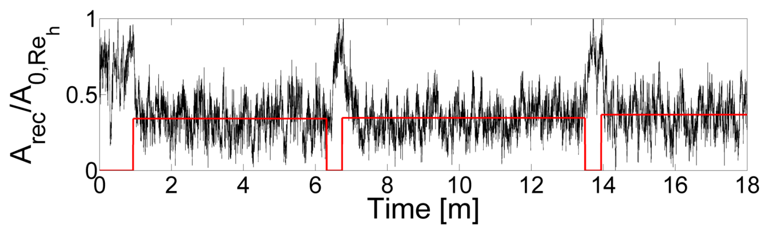


(d) Evolution of $A_{rec}$ as a function of time. Time-series are normalized by the uncontrolled recirculation area for the corresponding Reynolds number $A_{0,Re_h}$. Mean values of the controlled signal are shown in red. They are computed for each period when $Re_h$ is changed.

Fig. 4 Example of frequency-lock reactive control. From [7]

To demonstrate the efficiency of the frequency-lock approach, the free-stream velocity is randomly varied. The variations in $Re_h(t)$ (based on $u_{check}(t)$) are shown in figure 4a. A wide range of Reynolds numbers is explored (from $Re_h = 1400$ to 2400) to ensure strong variations in the shedding frequency. Figure 4b shows that the shedding frequency is evaluated each time the Reynolds number is changed. Figure 4c displays the evolution of jet to cross-flow velocity ratio amplitude $a_0$. It is interesting to notice that its optimal value is constant and close to 1.2. Finally, figure 4d shows the evolution of $A_{rec}(t)$ normalized by the uncontrolled value $A_{0,Re_h}$. Its mean value is also computed over each controlled phase (red lines on figure 4d). Re-computation only occurs for major changes in $u_{check}$. What constitutes a major change is defined by the user. Because shedding frequency is locked to actuation frequency, control is successful even when natural shedding frequency slightly varies. When controlled the recirculation area is reduced to 70 % up to 85 % of its uncontrolled value.

## 5 Closed-loop separation control using machine learning

### 5.1 Machine Learning Control approach

A generic and model-free approach to closed-loop control of nonlinear systems is proposed, referring to this approach as machine learning control (MLC) [5, 8]. Control laws are optimized with regards to a problem specific objective function using genetic programming [10]. Thus the principle is as follows: a first generation of control law candidates $b_i^1(s)$, called individuals ($b_i^1(s)$ is the $ith$ individual of the first generation), is randomly generated by combining user-defined functions (sin, cos, exp, log and tanh), constants and a sensor value $s$, giving $b = f(s)$. Each individual is evaluated yielding a value for a cost function $J$. The lower is $J$, the best the individual is. A new population $b_i^2$ is then generated by evolving the first generation. The figure 5 summarizes the procedure, which is iterated until either a known global minimum of $J$ is reached or the evolution is stalled.

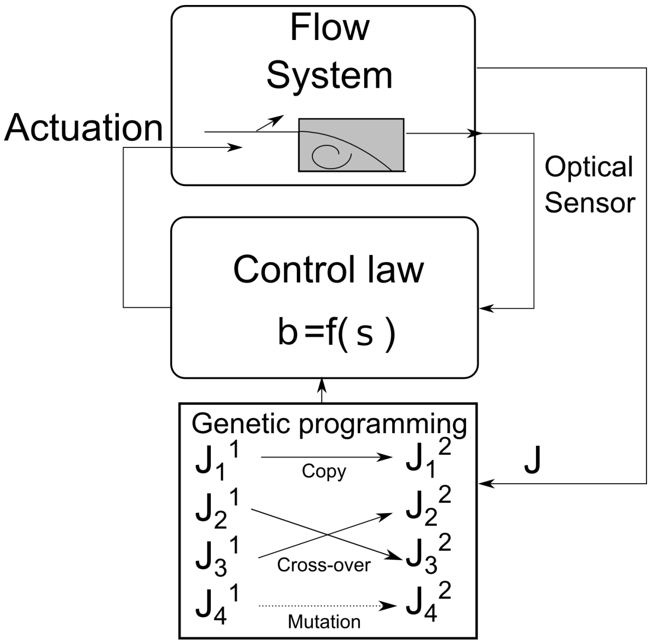


Fig. 5 Control loop featuring genetic programming. Control laws $b(s)$ are evaluated by the flow system. This is done over several generations of individuals. New generations are generated by replication, cross-over and mutation $J_i^n$ refers to the $i^{th}$ individual of generation $n$. From [8].

### 5.2 Closed-loop separation control parameters

As the diversity of the individuals is a key parameter of evolving algorithms, 500 different individuals are evaluated for each generation. This number of individuals is a good compromise between performance and testing time. Because the Reynolds number is kept constant to $Re_h = 1350$ for this experiment, the control is based on the jet velocity amplitude $U_j$. Thus $b = U_j/U_{j,max}$ is chosen as the control parameter with $U_{j,max}$ the maximum jet velocity. The state of the flow is evaluated with the normalized instantaneous recirculation area $s(t) = A_{rec}(t)/A_{0,Re_h}$. Finally the cost function $J$ for the individual $i$ is build as follows:

$$J(i) = (\langle s \rangle_T + w \langle |b_i| \rangle_T^2) > 0 \tag{3}$$

where $w$ is a penalty coefficient for the controller and $\langle - \rangle_T$ stands for the time-averaging over the evaluation time $T$. The reference is the value when the flow is uncontrolled: $J = 1$. $w$ qualifies the priority the user gives either to the gain on area reduction ($w < 1$) or to the actuation cost ($w > 1$). We set $w = 3/2$ to avoid high energy consumption, according to the results of open-loop control presented in [6]. $T = 1$ min is enough to get significant statistics to efficiently evaluate J: 2 generations are evaluated in approximately 24 hours.
A pre-evaluation of each control law is performed before application. This aims at discarding the functions leading to the saturation of the actuator.

### 5.3 Results

After 8 generations, the performance of the best individuals appear to converge and after 12 generations the best control law, called $b = K(s)$, is given by:

$$b = \exp -0.1138 \times \log(\cos(\log(s)) - \sin(\cos(\tanh(\sin(s))))). \tag{4}$$

for $J = 0.42$.

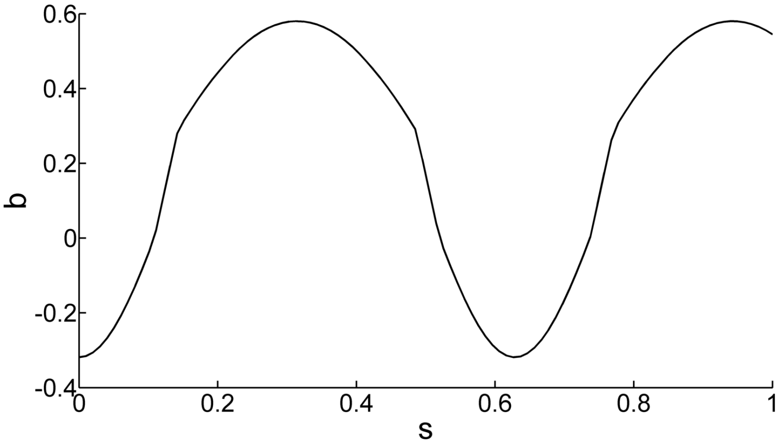


Fig. 6 Graph of the best control law $b = K(s)$ given in equation (4) obtained after 12 generations. From [8].

Figure 6 shows how $b$ depends on $s$ and the existence of two similar maxima $b \approx 0.6$ (injection) and two similar minima $b \approx -0.3$ (suction). Such curve reveals that a linear process could not give $K$. To go from an uncontrolled recirculation bubble ($s \sim 1$) to the best area reduction ($s \sim 0$), a first jet injection at high amplitude is carried out, followed by a strong suction then an injection again. Finally the post-transient regime ($s < 0.32$) is reached and $b$ is roughly an affine function of $s$.

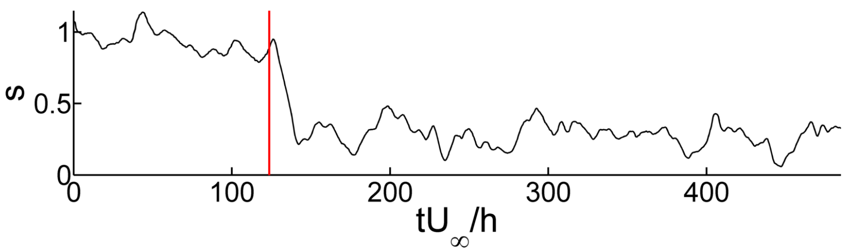


(a)

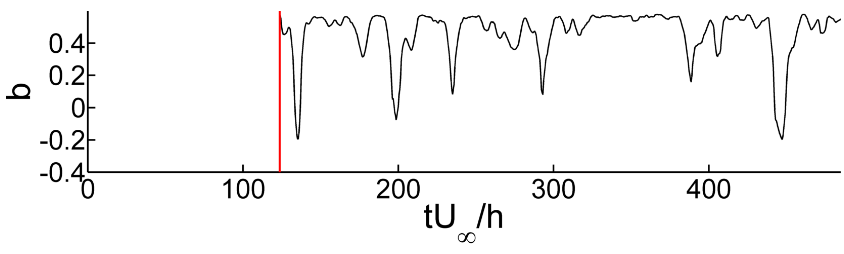


(b)

Fig. 7 (a) System response $s$ to the control law, the vertical line shows when control starts at $t = 120$. (b) Corresponding actuation $b$. From [8].

The results of $K$ are observed on the figures 7a and 7b which respectively give the time-series of the system response $s(t)$ to the control law and the corresponding action of the controller $b(t)$. Once activated (vertical line), $K$ keeps a reduction of the recirculation area between 50 % and 80 %.
The feedback-loop creates oscillations at 0.1 Hz, close to the flapping frequency of the recirculation bubble as the frequency analysis shows it in figure 8. According to [11], this frequency is typically an order of magnitude

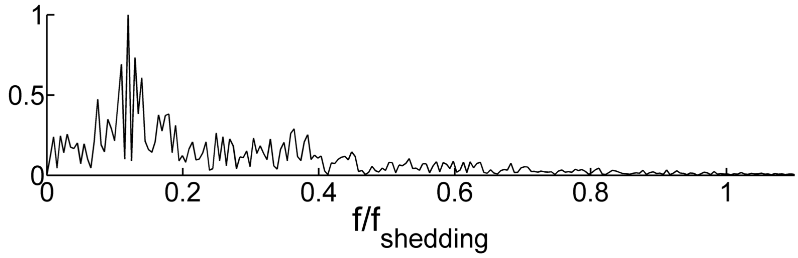


Fig. 8 Normalized frequency spectrum obtained by Fourier transform of the actuation signal, frequency is normalized by vortex shedding frequency. From [8].

lower than the shear layer shedding frequency, close to 1 Hz at this Reynolds number. The choice of the instantaneous recirculation area as input and the natural flapping frequency are most likely the reasons of this 0.1 Hz feedback dynamics.
Finally the control law $K$ is tested at different Reynolds numbers. Since the recirculation area is directly considered in the controller action, the actuator adapts well to these operating conditions variations, giving $J = 0.33$ for $Re_h = 900$ and $J = 0.59$ for $Re_h = 1800$. In order to keep a low cost function, an improvement of the MLC law could be to also take the jet to cross-flow momentum ratio dependence on $Re_h$ into account.

## 6 Conclusion

By using real-time PIV, two control laws were obtained to minimize the recirculation on a backward-facing step flow. Even if they have been based on different properties of the BFS flow - the frequency-lock reactive control exciting the Kelvin-Helmholtz frequencies while the model-free MLC approach exploits the flapping frequency - both gives successful results. A real-time measure of the recirculation area has been efficiently and robustly linked to actuation values, leading to an 80 % reduction of the recirculation area. The main difference between both control methods lies in their possible applications. Whereas the frequency-lock control needs to know the timescales involved in the relevant flow processes, the MLC approach can be used on flows whose all geometry specifications can not be experimentally studied, such as a detailed vehicle model. The MLC approach requires a huge amount of velocity fields to find a satisfactory convergence. Using real-time PIV allows for handling large amount of statistical data without having to store the corresponding thousands instantaneous velocity fields. It also makes parametric studies easier as we have an instantaneous access to the data of interest characterizing the state of the flow. It even becomes easier to run the experiments rather than storing the data. It is also possible to run such an algorithm with very cheap set-ups. For all these reasons, we believe Real-Time PIV should become very popular in the next years.

## References

[1] Le Besnerais G and Champagnat F (2005) Dense optical flow by iterative local window registration. In: ICIP (1), pp 137:140.

[2] Cambonie T, Gautier N and Aider J L (2013) Experimental study of counter-rotating vortrex pair trajectories induced by a round jet in cross-flow at low velocity ratios. *Experiments in Fluids*, vol. 54, pp 1-13.

[3] Champagnat F, Plyer A, Le Besnerais G, Leclaire B, Davoust S and Le Sant Y (2011) Fast and accurate PIV computation using highly parallel iterative correlation maximization. *Experiments in Fluids*, vol. 50, pp 1169-1182.

[4] Chung K B and Sung H J (1996) Control of turbulent separated flow over a backward-facing step by local forcing. *Experiments in Fluids*, vol. 21, pp 417-426.

[5] Duriez T, Parezanović V, Laurentie J C, Fourment C, Delville J, Bonnet J P, Cordier L, Noack B R, Segond M, Abel M W, Gautier N, Aider J L, Raibaudo C, Cuvier C, Stanislas M and Brunton S (2014) Closed-

loop control of experimental shear layers using machine learning (invited). In: 7$^{th}$ AIAA Flow Control Conference, pp. 1-16. Atlanta, Georgia, USA.

[6] Gautier N. and Aider J.-L. (2014) Upstream open-loop control of the recirculation area downstream of a backward-facing step. Comptes Rendus Mécanique (CRAS II B), 342 (6), pp 382-388.

[7] Gautier N. and Aider J.-L. (2015a) Frequency-lock reactive control of a separated flow enabled by visual sensors. *Experiments in Fluids*, vol. 56, pp 16. doi: 10.1007/s00348-014-1869-3.

[8] Gautier N., Aider J.-L., Duriez T, Noack B R, Segond M and Abel M (2015b) Closed-loop separation control using machine learning. *Journal of Fluid Mechanics*, 770, pp 442 - 457.

[9] Gautier N. and Aider J.- L. (2015c) Real-time planar flow velocity measurements using an optical flow algorithm implemented on GPU. *Journal of Visualization*, vol. 18 (2), pp 277 - 286.

[10] Koza J R, Bennett III F H and Stiffelman O (1999) Genetic Programming as a Darwinian Invention Machine. In: Lecture Notes in Computer Science, vol. 1598, ed. Springer.

[11] Spazzini P G, Luso G, Onorato M, Zurlo N and Di Cicca G M (2001) Unsteady behavior of a back-facing step. *Experiments in Fluids*, vol. 30, pp 551-561.